NJC

Accepted Manuscript

This is an *Accepted Manuscript*, which has been through the Royal Society of Chemistry peer review process and has been accepted for publication.

Accepted Manuscripts are published online shortly after acceptance, before technical editing, formatting and proof reading. Using this free service, authors can make their results available to the community, in citable form, before we publish the edited article. We will replace this *Accepted Manuscript* with the edited and formatted *Advance Article* as soon as it is available.

You can find more information about *Accepted Manuscripts* in the Information for Authors.

Please note that technical editing may introduce minor changes to the text and/or graphics, which may alter content. The journal's standard Terms & Conditions and the Ethical guidelines still apply. In no event shall the Royal Society of Chemistry be held responsible for any errors or omissions in this *Accepted Manuscript* or any consequences arising from the use of any information it contains.

ROYAL SOCIETY OF CHEMISTRY

www.rsc.org/njc

Journal Name

ARTICLE

Synthesis and Acid-Base Property of Proton-Bridged Biaryl Compound Based on Pyridylazulene

Received 00th January 20xx,
Accepted 00th January 20xx

DOI: 10.1039/x0xx00000x

www.rsc.org/

Kazuki Ninomiya[a], Yumi. Harada[b], Tomoaki Kanetou,[c] Yuma Suenaga,[a] Toshihiro Murafuji[a] and Ryo Tsunashima[c]

Herein, we report the synthesis of 1,1′-bi(2-pyridylazulene) (**1**), in which pyridyl moieties were coupled to a biaryl framework for hydrogen bonding between the two aryl skeletons. The two 2-pyridylazulene moieties in **1** were linked through facile aryl–aryl coupling between the 1- and 1′-positions of the azulene skeletons, where 1-haloazulene was stabilized by electron withdrawing pyridyl substitution. In addition, single crystals of the mono-protonated species (**1H**$^+$) were successfully obtained as the BF_4^- salt. X-ray diffraction analysis at 153 K revealed an intramolecular hydrogen bond between the two pyridyl moieties, giving a racemic mixture of axial chiral species. DFT calculations were performed to understand the hydrogen bonding structure and an almost single minimum potential for thermal proton motion was suggested. The acid–base characteristics were investigated in acetonitrile and **1** was revealed to exhibit two-step protonation of its pyridyl moieties. By comparison with monomeric 2-pyridylazulene, the stronger basic character of **1** was confirmed. This is ascribed to the macrocyclic effect of the two pyridyl moieties bridged by a proton, as seen in the single crystal of **1H**$^+$. Furthermore, two different energy shifts associated with intramolecular transition were observed under protonation; the first protonation produced a blue shift in the absorption maximum, whereas a red shift was observed for the second protonation. The unusual blue shift was explained by stabilization of the HOMO owing to an extended electronic structure between the two azulene skeletons. This unique steric structure was achieved by proton bridging in the pyridyl-substituted biaryl compound.

Introduction

The exploration of organic π-conjugated molecules is a developing issue for organic electronics.[1] Huge efforts have been made to achieve π-conjugated molecules that exhibit electrical, optical, and magnetic properties, as well as switching phenomena and/or multi-functionality.[2-12] Among the π-conjugated molecules, azulene, which is an isomer of naphthalene, has been regarded as an important active component whose characteristics have been developed by coupling with other functional organic molecular systems. Azulene derivatives have been included in organic field-effect transistors, charge-transfer complexes, nonlinear optics, and sensing applications.[13-17] The relevant phenomena are considered a consequence of the non-zero dipole moment of the azulene skeleton, which consists of a cyclopentadienyl anion and tropylium cation. In addition, the energy gap between the highest occupied molecular orbital (HOMO) and lowest unoccupied molecular orbital (LUMO) of azulene is small. As the unique electronic systems of azulene are distinct from other π-conjugated molecules, reactions to obtain comprehensive derivations of the azulene skeleton have also been explored.[18-23] Among these derivatives, biaryl compounds, such as 1,1′-biazulene, are expected to be isomers of 1,1′-binaphthyl compounds with unique electronic systems. However, only limited synthetic routes have been reported for aryl–aryl coupling of azulene,[18-20] most likely owing to the intrinsic instability of 1-haloazulene for the coupling reaction.

Pyridine is another π-conjugated molecule that exhibits basic characteristics through a lone pair on the N atom. The hydrogen bonding structure influences the electronic nature of pyridine; for example, the electron withdrawing ability was enhanced through protonation. Pyridyl-substituted extended π-systems have unique electronic characteristics. For example, the π-donor tetrathiafulvalene substituted with pyridine changes its electronic structure according to its protonation state. The HOMO–LUMO gap showed a red shift of ca. 130 nm with protonation.[24] Owing to an interest in molecular-based multi-functional systems and switching ability, a system comprising a dynamic proton coupled with an extended electronic structure has been explored. Hydrogen bonds can function as an antenna for stimulus because their energy corresponds to room temperature. Hydrogen-bond-dynamics-based switching of conductivity and magnetism were realized using catechol-fused ethylenedithiotetrathiafulvalene.[25]

[a] Graduate School of Medicine, Yamaguchi University, Yamaguchi 753-8512, Japan
[b] Department of biology and chemistry, Yamaguchi University, Yamaguchi, 753-8512, Japan.
[c] Graduate School of Science and Engineering, Yamaguchi University, Yamaguchi 753-8512, Japan.

† Electronic Supplementary Information (ESI) available: details of spectra and DFT calculation. See DOI: 10.1039/b000000x/

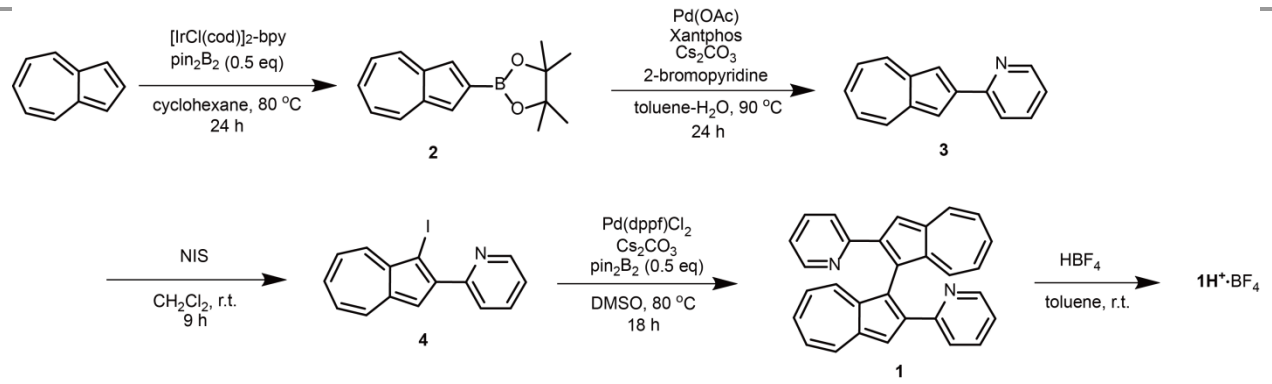

Scheme 1. Synthetic scheme of **1** and **1H**$^+$·BF_4

Pyridine-substituted azulene derivatives were also reported to show interesting chromic characteristics according to structure around the N atoms, such as protonation and metal coordination.[26]

From these points of views, we have investigated the synthesis of 1,1′-bi(2-pyridylazulene) (**1**) and its protonated structure. The molecule is an azulene-based biaryl compound with two pyridyl moieties substituted at the 2-positions of the azulene skeletons. Compound **1** was prepared from azulene by a four-step reaction with a total yield of 25%. The electron withdrawing ability of the pyridyl moiety was deduced to stabilize 1-haloazulene for facile aryl–aryl coupling to obtain compound **1**. Single crystals of the mono protonated species (**1H**$^+$) were successfully obtained, and crystallographic structural analysis revealed an intramolecular hydrogen bond between the two pyridyl moieties, giving a racemic mixture of axial chiral species. The acid–base characteristics in solution indicated that **1** has a stronger basic character than monomeric 2-pyridylazulene owing to a macrocyclic effect. The first and second protonation processes resulted in blue and red shifts of the absorption maximum, respectively. Our insight shows that intramolecular proton bridge between bipyridyl groups behave as a chelating ligand to accommodate proton in solution, followed to stabilization of a unique steric structure.

Results and discussion

Synthesis

Compound **1** was synthesized from azulene in four steps with a total yield of 25% (Scheme 1). Compound **3** was synthesized based on a method reported previously.[26] The experimental details of the syntheses of **2** and **3** are included in the ESI. Azulene was reacted with 0.5 equiv bis(pinacolato)diboron (pin_2B_2) in the presence of an Ir-catalyst to form compound **2**. Suzuki coupling with 2-bromopyridine provided compound **3** (yield 83%). The reaction of **3** with *N*-iodosuccinimide resulted in iodination at the 1-position, yielding compound **4** (yield 80%). Even though 1-haloazulenes are usually unstable,[20] compound **4** was stable in air. This stability is ascribed to the electron withdrawing ability of the pyridyl moiety at the 2-position of azulene. Compound **1** was obtained by borylation of **4** using 0.5 equiv pin_2B_2 (yield 52%). Formation of **1** was considered to occur through Suzuki coupling of unreacted **4** and borylated **4**. A toluene solution of **1** was reacted with HBF_4, yielding blue single crystals after repeated recrystallization from dichloromethane–hexane (2:3).

Crystal Structure

Single crystals of compound **1H**$^+$ were isolated as the BF_4^- salt. SC-XRD analysis of **1H**$^+$·BF_4 at 153 K showed that the salts were crystallized in a triclinic system with space group *P*-1, a = 13.677(7) Å, b = 16.455(8) Å, c = 19.539(8) Å, α = 70.956(18)°, β = 76.30(2)°, γ = 87.68(2)°, V = 4035(3) Å^3, and Z = 2. Crystal structure determination revealed that the racemic crystals contain both axial chiral enantiomers in a 1:1 ratio, resulting in a total of six independent **1H**$^+$ cations. The crystal also contains two toluene molecules and a certain number of crystalline water molecules that could not be determined owing to their large disorder. In air, the single crystals easily lost the high crystallinity required for XRD analysis owing to facile evaporation of the solvent molecules. Therefore, the single crystal was mounted quickly onto a goniometer for measurement at 153 K. In addition, some BF_4^- counter cations were also disordered.

Structure of 1H$^+$ cations. Figure 1 shows the structure of **1H**$^+$ cations. We have labeled the cations as **1H**$^+$**-a** (contains N1 and N2 atoms), **1H**$^+$**-b** (contains N3 and N4 atoms), and **1H**$^+$**-c** (contains N5 and N6 atoms). The interatomic distances between the N atoms on the two pyridyl moieties (d_{NN}) are 2.647, 2.614, and 2.643 for **1H**$^+$**-a**, **1H**$^+$**-b**, and **1H**$^+$**-c**, respectively. These distances are shorter than the sum of van der Waals (vdW) radii of N atoms, indicating a hydrogen bond through a proton positioned between the two N atoms. These three cations have similar interatomic distances. The dihedral angles (ψ) between the pyridine (Py) and azulene (Az) rings are summarized in Table 1, where the numbers n correspond to the atomic number of the N atom in Figure 2. In contrast to similar interatomic distances in the cations, the dihedral angles between the rings are significantly different. The structural independence of **1H**$^+$**-a**, **1H**$^+$**-b**, and **1H**$^+$**-c** could originate from differences in the intermolecular interactions in the crystal.

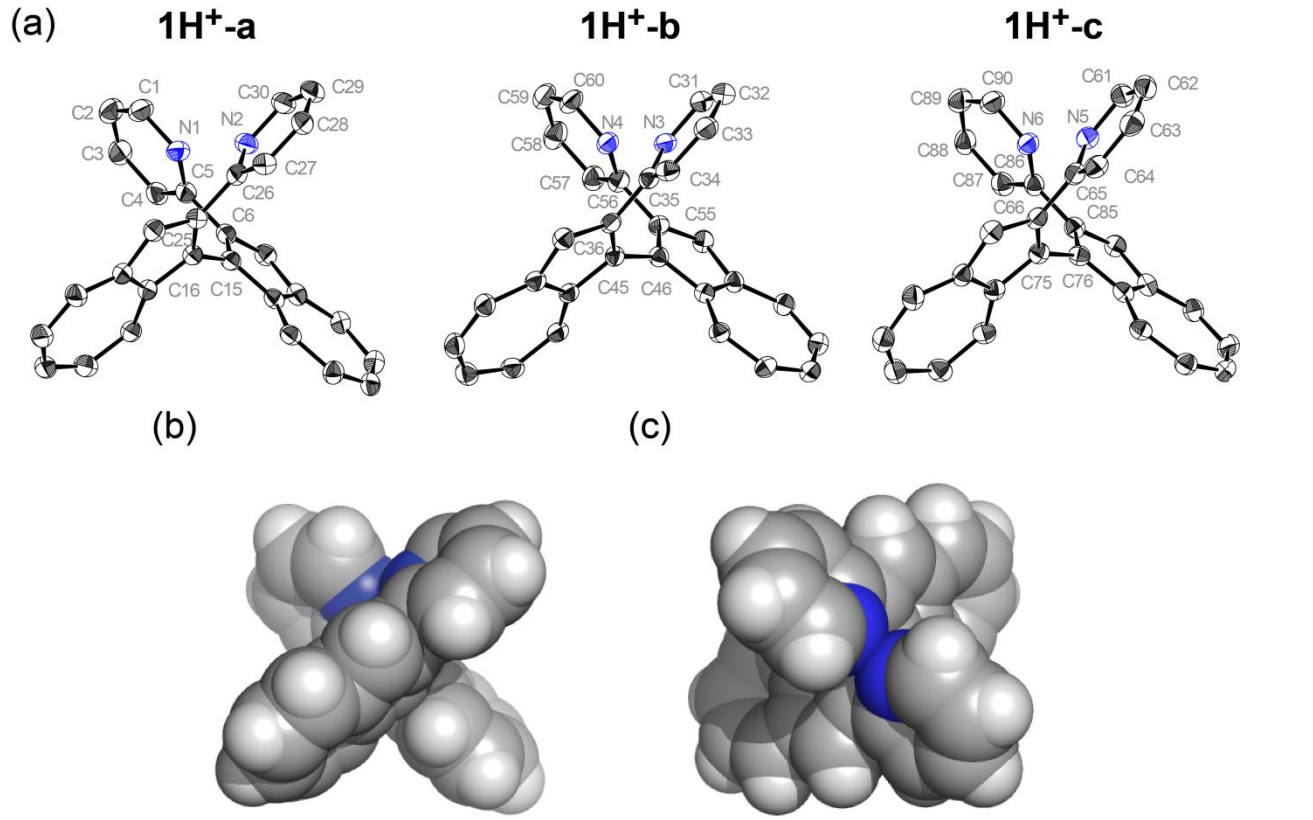

Figure 1. (a) ORTEP drawings of **1H**$^+$ molecules. Hydrogen atoms are omitted for clarity, and thermal ellipsoids are set to 30% probability (with atomic numbers shown for selected atoms). Space filling drawings of **1H**$^+$**-a** (C: gray, H: white, and N: blue) along the (b) same and (c) normal direction to Figure 1a.

Intermolecular interactions. The molecular packing was analyzed using Hirshfeld surfaces. The normalized intermolecular distances (d_n) were plotted on the Hirshfeld surface of the molecule under consideration with positive values (colored blue) representing intermolecular distances larger than the sum of the vdW radii (negative surfaces are colored red).[27-28] Figure 2 shows the Hirshfeld surface of **1H**$^+$**-a**, **1H**$^+$**-b**, and **1H**$^+$**-c**. Interactions were observed for **1H**$^+$**-a**, **1H**$^+$**-b** and **1H**$^+$**-c**, indicated by reddish areas on the Hirshfeld surfaces (smaller than the sum of the vdW radii), with different types of interactions for each **1H**$^+$. Among them, strong H···F interaction between **1H**$^+$ and BF_4^- were observed. Furthermore, CH–π interactions between **1H**$^+$ molecules and weak face-to-face π–π interactions were also observed. The different intermolecular interactions in **1H**$^+$**-a**, **1H**$^+$**-b**, and **1H**$^+$**-c** are considered to be the origin of crystallographic independence.

DFT calculations

Details of the hydrogen bonds were examined using DFT calculations. The dependence of the N···H distance on the potential energy difference (ΔE) and molecular orbitals was calculated using the B3LYP/6-31G(d,p) level of theory.

The structure was taken from the crystal structure by removing the azulene rings. The coordinates of the proton were changed between the two N atoms, where the NHN angle was fixed at 180°. The differential distance from a center was Δd, where ΔE at Δd = 0 was set to 0 eV. Figure 3 shows the ΔE - Δd curves estimated for each molecule. Both **1H**$^+$**-a** and **1H**$^+$**-c** showed an asymmetric but shallow double minimum potential with an activation energy of 0.05 eV. However, these structural differences could arise from the thermal vibrations of the molecules. A single minimum potential is considered to correspond to an intrinsic structure, as seen for **1H**$^+$**-b** where the proton is thermally disordered with a displacement range of ca. 0.4 Å.

Table 1. Structural data of **1H**$^+$ cations determined by SC-XRD analysis.

molecules	**1H**$^+$**-a**	**1H**$^+$**-b**	**1H**$^+$**-c**
d_{NN}/Å	2.643	2.611	2.637
ψ/°	46.53 (Py1-Az1)	45.40 (Py3-Az3)	51.49 (Py5-Az5)
	44.92 (Py2-Az2)	47.35 (Py4-Az4)	51.98 (Py6-Az6)
	86.17 (Az1-Az2)	89.84 (Az3-Az4)	88.14 (Az5-Az6)
	72.48 (Py1-Py2)	73.47 (Py3-Py4)	68.67 (Py5-Py6)

ψ; dihedral angles between two rings

Sets of molecular orbitals were calculated for **1H**$^+$**-a** (Δd = -0.2, 0, and 0.2 Å) and **1H**$^+$**-b** (Δd = 0 and 0.2 Å) using the full structures obtained by SC-XRD analysis (for details, see Table S3-3-1 and S3-3-2). The orbital distributions were very similar for **1H**$^+$**-a** and **1H**$^+$**-b**.

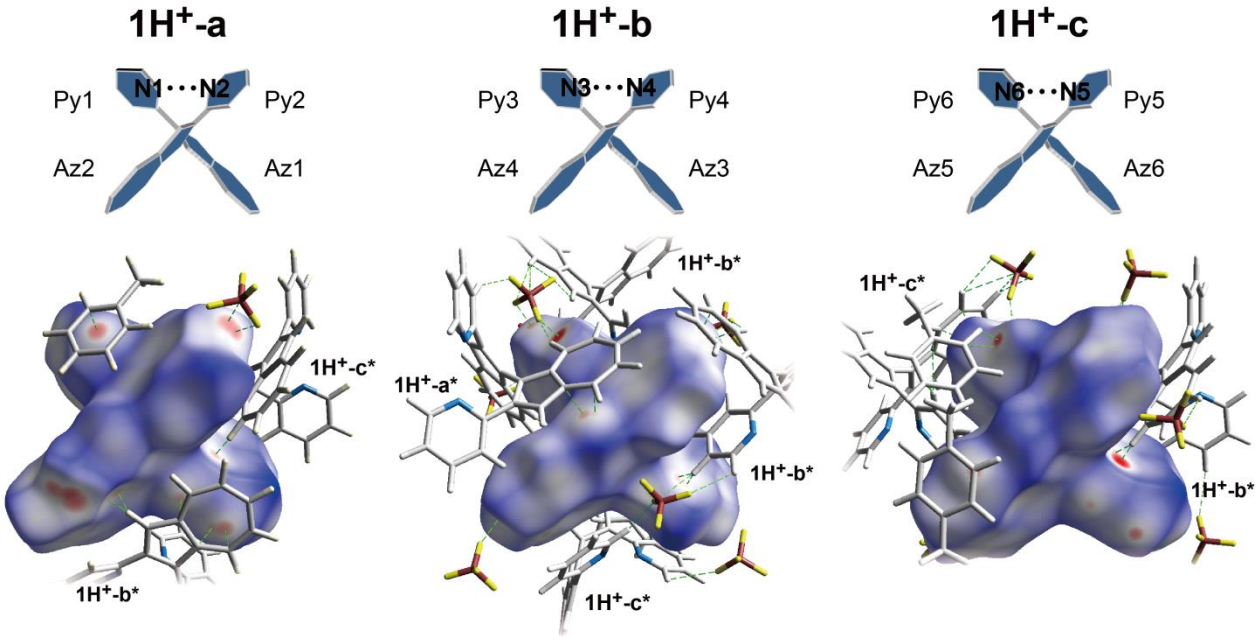

Figure 2 Hirshfeld surfaces of respective **1H**$^+$ molecules. Molecules are viewed along the same direction shown in Figure 1 (Hirshfeld surface of molecule under consideration was shown. Green dotted lines represented intermolecular interaction) and crystalline water molecules are omitted. The enantiomers are indicated with an asterisk (*).

The HOMO was mainly distributed over the two azulene rings through the C–C aryl–aryl linkage between the 1-positions of the 2-pyridylazulene moieties.

This distribution, as well as the energy level, did not depend on the proton displacement in either **1H**$^+$**-a** or **1H**$^+$**-b**. In contrast, the LUMO was dependent on the position of the proton. The LUMO was mainly located on the pyridylazulene skeleton to which the proton was closest. The LUMO was stabilized by the proton, which was enhanced by the electron withdrawing ability of the pyridine ring. The LUMO energy at Δd = 0 (-5.061 eV) decreased by 0.2 eV at Δd = ±0.2 Å for **1H**$^+$**-a**.

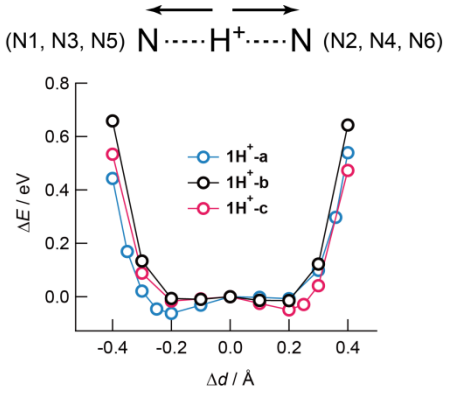

Figure 3. Plots of N–H distance (Δd) and potential energy difference (ΔE) for **1H**$^+$**-a** (blue), **1H**$^+$**-b** (black), and **1H**$^+$**-c** (red). Positive Δd indicates that the proton is positioned closer to N2, N4, and N6 in **1H**$^+$**-a**, **1H**$^+$**-b**, and **1H**$^+$**-c**, respectively.

Protonation processes in solution

The vis-NIR spectra in solution (0.5 mM in acetonitrile) of **1** and, as a control experiment, 2-pyridylazulene (**3**) were monitored during titrations with trifluoroacetic acid (TFA) (Figure 4).

Absorption bands attributed to intramolecular transitions of **1** were observed at 604 and 651 nm with a shoulder at 720 nm. The acidification of **1** resulted in increases in the absorbance at 594, 625, and 690 nm accompanied by a decrease in the shoulder at 720 nm. This blue shift was observed up to 1 equiv of TFA. Further acidification caused the bands to red shift. The absorbance at 646 nm increased and saturation was observed above 200 equiv of TFA. This two-step acid–base reaction was explained by the existence of two pyridyl moieties in **1**.

$$\mathbf{1} + \mathrm{H}^+ \rightleftharpoons \mathbf{1H}^+ \quad K_{11} = \frac{[\mathbf{1H}^+]}{[\mathbf{1}][\mathrm{H}^+]} \qquad (1)$$

$$\mathbf{1H}^+ + \mathrm{H}^+ \rightleftharpoons \mathbf{1H_2}^{2+} \quad K_{12} = \frac{[\mathbf{1H_2}^{2+}]}{[\mathbf{1H}^+][\mathrm{H}^+]} \qquad (2)$$

The equilibrium constants log K_{11} and log K_{12} estimated from the spectral changes were 4.3 and 1.8, respectively (Figure 4c and d).

Compound **3** also possess a pyridyl moiety with basic characteristics.[26] Absorption bands attributed to intramolecular transitions of **3** were observed at 582 and 627 nm with a shoulder at 687 nm. Acidification of **3** led to an increase in the absorbance at 598, 633, and 690 nm, with an accompanying red shift, similar to the second protonation of **1**.

Journal Name

ARTICLE

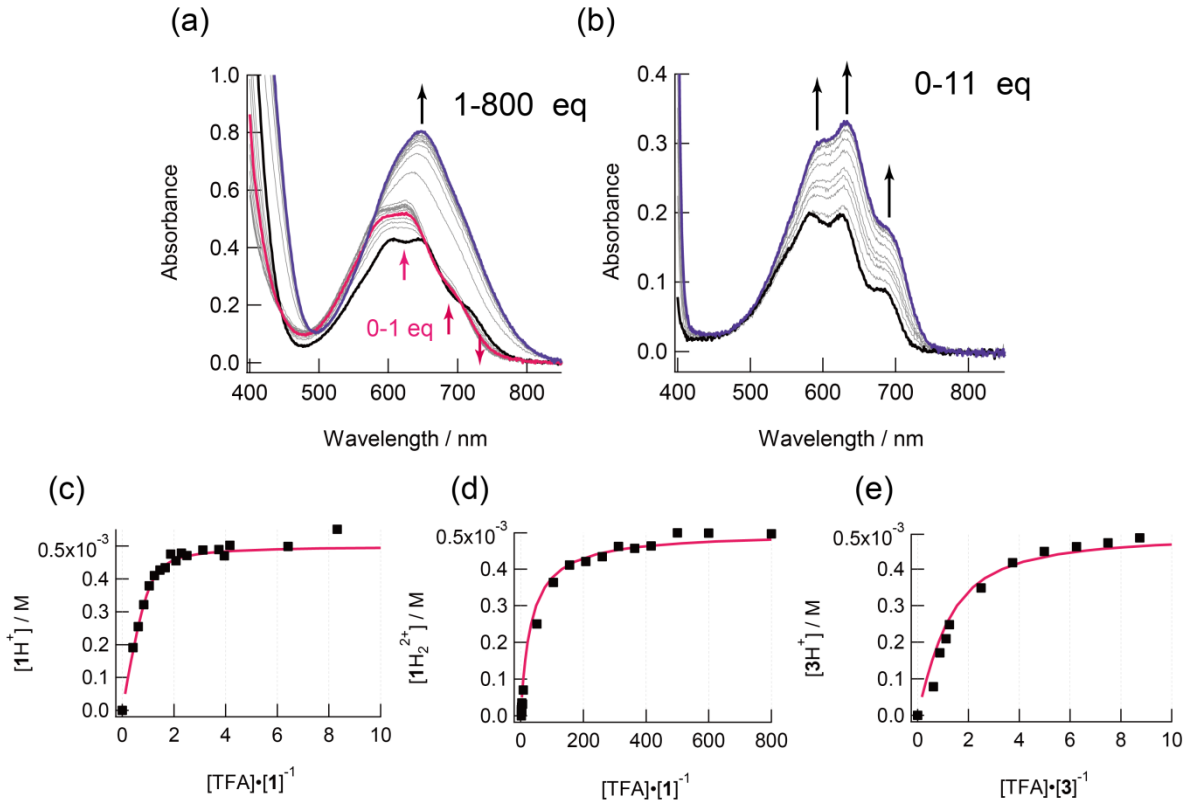

Figure 4. Electronic absorption spectral changes during titrations of (a) **1** (bold black, pink, and blue lines correspond to 0, 1, and 800 equiv of added protons, respectively) and (b) **3** (0.5 mM in acetonitrile) with TFA. The changes in concentration of $\mathbf{1H^+}$, $\mathbf{1H_2^{2+}}$, and $\mathbf{3H^+}$ with proton equivalents per **1** or **3** are shown in (c), (d) and (e), respectively. Concentration of components were estimated from absorbance at 606 nm for **1** and 700 nm for **3**.

Corresponded spectroscopic changes have been reported using different solvent system.[26] Figure 4e shows the concentration of $\mathbf{3H^+}$ estimated from the changes in the absorbance. The protonation of **3** was saturated at a higher proton concentration than that for **1**.

$$\mathbf{3} + \mathrm{H^+} \rightleftharpoons \mathbf{3H^+} \qquad K_{31} = \frac{[\mathbf{3H^+}]}{[\mathbf{3}][\mathrm{H^+}]} \qquad (3)$$

The equilibrium constant log K_{31} was estimated as 3.5. The enhanced basic characteristics of **1** indicate that the intramolecular hydrogen bond results in a macrocyclic chelate effect. The structure of the mono-protonated species in acetonitrile corresponds to that characterized by crystallographic analysis of $\mathbf{1H^+}$.

The first protonation of **1** resulted in a blue shift of the bands, even though red shifts were observed for the other protonation processes ($\mathbf{1H^+}$ to $\mathbf{1H_2^{2+}}$ and **3** to $\mathbf{3H^+}$). It has been reported for **3** that the red shift originates from the stabilization of the LUMO of the azulene skeleton, which has a large coefficient at the 2-position in the LUMO. This is because of the electron withdrawing ability of the pyridyl moiety.[26]

The red shift observed for the second protonation of **1** is ascribed to the similar decrease of the LUMO energy. The LUMO is contributed by the 2-pyridylazulene skeleton closest to the proton (Table S3-3-1). In contrast, the blue shift observed for the first protonation of **1** was attributed to stabilization of the HOMO of the azulene skeleton, where the stabilization is greater than the decrease in the LUMO energy owing to protonation. The azulene skeleton has large coefficients at the 1-position in the HOMO. By proton bridging between the two 2-pyridylazulene skeletons, molecular rotation was fixed to form an axial chiral structure. The DFT calculations showed that the HOMO is distributed over both the azulene moieties through the aryl–aryl bond. This implies a decrease of the HOMO energy in the proton-bridged structure compared with a steric structure where the two 2-pyridylazulene skeletons are electronically isolated from each

other. This unique proton-bridged structure is considered to be stable, even in acetonitrile solution, and the steric conformation is accompanied by stabilization of the HOMO owing to extension of the orbital over both azulene skeletons.

Conclusions

In summary, we have reported the synthesis of compound **1**, its acid–base characteristics, and the structure of the protonated species. Compound **1** was synthesized by aryl–aryl coupling of the monomeric compound **3**, where enhanced stability of the 1-haloazulene derivative was obtained by substitution with the electron withdrawing pyridyl moiety at the 2-position. Furthermore, single crystals of the protonated species (**1H$^+$**) were obtained. The X-ray diffraction analysis revealed that **1H$^+$** was crystallized as a racemic mixture of axial chiral species consisting of six independent molecules: **1H$^+$-a**, **1H$^+$-b**, and **1H$^+$-c** and their enantiomers. DFT calculations based on the crystal structure showed an almost single minimum potential for displacement of the proton between the two N atoms. Compound **1** showed a two-step protonation reaction in acetonitrile that originated from the two pyridyl moieties. The first step from **1** to **1H$^+$** showed stronger basic characteristics than that of 3. This is ascribed to a macrocyclic chelate effect in 1 owing to a proton bridge between the two pyridyl moieties. The first and second protonations of **1** resulted in blue and red shifts of the absorption bands, respectively, which were understood using DFT calculations. The LUMO has a large coefficient at the 2-position of the azulene skeleton, whereas the HOMO has a large coefficient at the 1-position. The first protonation of the pyridyl moiety at the 2-position resulted in decreases in both the HOMO and LUMO energies. This is because the distribution of the HOMO was extended over both azulene skeletons when the molecular conformation was fixed by a proton bridge. The observed blue shift implies that the stabilization of the HOMO exceeded that of LUMO when the intramolecular hydrogen bond was formed. In contrast, the second protonation broke the intramolecular proton bridge and the HOMO was no longer stabilized; therefore, the decrease in the LUMO energy caused a red shift of the absorption band. Compound **1** realizes a unique steric structure by proton bridging between the 2-pyridylazulene skeletons. Further developments and separation of the axial chiral species are expected through formation of metal complexes with compound **1** as a ligand or saltation with chiral anion.

Experimental

General procedures

All ^{1}H and ^{13}C NMR spectra were recorded using Bruker AVANCE 400s. The chemical shifts are described as values in ppm relative to a $Si(CH_3)_4$ standard for ^{1}H NMR. Mass spectra and IR spectra were taken by using Bruker micrOTOF II and Thermo Fisher Scientific avatar 370 (KBr pellets), respectively. All reactions were performed under Ar.

Synthesis

Synthesis of 1-iodo-2-(2-pyridyl)azulene (4). A dichloromethane solution of **3** (8.6 mmol, 200 mL) was mixed with *N*-iodosuccinimide (9 mmol) in an ice bath. After stirring at room temperature for 9 h, a saturated aqueous solution of sodium hydrogen carbonate was added to the reaction mixture, which was then extracted with dichloromethane (distilled, 200 mL × 1, 10 mL × 2). The solution was dried over anhydrous sodium sulfate, filtrated, and concentrated, followed by chromatography on silica gel with hexane–ethyl acetate (5:1) as the eluent to give the product. Green crystal; yield 87%; ^{1}H-NMR (400 MHz, $CDCl_3$) δ 7.25 (1H, t, J = 9.6 Hz), 7.29–7.33 (1H, m,), 7.35 (1H, t, J = 9.6 Hz), 7.64 (1H, t, J = 9.6 Hz), 7.83 (1H, td, J = 7.6, 1.6 Hz), 7.90 (1H, s), 8.10 (1H, dt, J = 8.0, 0.8 Hz), 8.30 (1H, d, J = 9.6 Hz), 8.46 (1H, d, J = 9.6 Hz), 8.81 (1H, dq, J = 4.4, 1.2 Hz). ^{13}C-NMR (100 MHz, $CDCl_3$) δ 74.7, 119.4, 122.5, 124.6, 124.7 (x2), 135.9, 137.3, 138.3, 140.2, 141.3, 141.4, 149.9, 150.17, 155.2. MS (*m/z*): 331.9940 ($C_{15}H_{11}IN^+$, 331.9931). FTIR (cm^{-1}): 1587 (w), 1562 (w), 1458 (w), 1421 (w), 1396 (w), 781 (s), 745 (w), 727 (w), 579 (w).

Synthesis of 2,2′-bis(pyridine-2-yl)1,1′-biazulene (1). A mixture of **4** (6.2 mmol), [1,1′-bis(diphenylphosphino)ferrocene]palladium(II) dichloride (10 mol%, 0.62 mmol), bis(pinacolato)diboron (3.1 mmol), and cesium carbonate (18.5 mmol) in dimethyl sulfoxide (50 mL) was heated at 90 °C for 18 h. After cooling to room temperature followed by addition of water, the mixture was extracted with ethyl acetate (10 mL × 3). The organic layer was dried over anhydrous sodium sulfate and filtered, followed by chromatography on silica gel with hexane–ethyl acetate (5:1) as the eluent to give the product. Green crystal; yield 52%; ^{1}H-NMR (400 MHz, $CDCl_3$) 6.74 (2H, d, J = 8.4 Hz), 6.91–6.96 (4H, m), 7.15–7.22 (4H, m), 7.51 (2H, t, J = 9.8 Hz), 7.77 (2H, d, J = 9.6 Hz), 8.25 (2H, s), 8.47 (2H, d, J = 9.6 Hz), 8.57 (2H, d, J = 4.0 Hz). ^{13}C-NMR (100 MHz, $CDCl_3$) δ 118.0, 121.9, 122.7, 123.2, 123.8 (x2), 136.1, 137.0, 137.8, 138.1, 140.5, 140.6, 148.7, 149.7, 154.8. MS (*m/z*): 409.1701 ($C_{30}H_{21}N_2^+$, 409.1699). FTIR (cm^{-1}): 1568 (s), 1425 (s), 1406 (s), 781 (s), 737 (s).

Crystallization of 1H$^+$·BF$_4$. Compound **1** was dissolved in 30 mL of toluene. After the addition of 0.70 mL of an aqueous solution of tetrafluoroboric acid (2%), the mixture was stirred for 30 min. The oily crude product was dissolved in dichloromethane, and then washed with water. The organic layer was dried over anhydrous sodium sulfate, concentrated, and recrystallized from dichloromethane–hexane (2:3) to yield blue single crystals suitable for single crystal X-ray diffraction (SC-XRD) analysis.

X-ray crystallography

The SC-XRD analysis of **1H$^+$**·BF_4 was performed using a Rigaku MERCURY diffractometer with graphite-monochromated Mo-Kα radiation. The data were collected at 153 K. The structure was solved by direct methods and expanded using Fourier techniques. A single crystal of **1H$^+$**·BF_4 contains two toluene molecules with static disorder. In addition, occupancies of disordered water molecules were defined as non-unit values.

Crystal data: [$\mathbf{1H}^+ \cdot BF_4$]·$2C_7H_8$·$/H_2O$ (I was not determined), $C_{100.5}H_{71.5}B_3F_{12}N_6O_{1.9}$, M = 1654.18, triclinic, a = 13.677(7) Å, b = 16.455(8) Å, c = 19.539(8) Å, α = 70.956(18)°, β = 76.30(2)°, γ = 87.68(2)°, V = 4035(3) Å^3, T = 153(2) K, space group P-1, Z = 2, μ(MoKα) = 0.1, 40023 reflections measured, 17603 independent reflections (R_{int} = 0.0780). The final R_1 values ($I > 2\sigma(I)$) were 0.1034. The final $wR(F^2)$ values ($I > 2\sigma(I)$) were 0.2693. The final R_1 values (all data) were 0.1586. The final $wR(F^2)$ values (all data) were 0.3137. The goodness of fit on F^2 was 1.314. CCDC number 1061580.

Measurements

The acid–base reaction of **1** in acetonitrile (0.5 mM) was monitored using a UV-vis-NIR spectrophotometer (JASCO V-670) through titration with CF_3COOH. Titration using HBF_4 resulted in similar changes (Figure S4). Peaks observed after protonation are almost corresponded. However, first and second protonation are almost overlapped. And spectra changes are saturated at 4 eq of acid. This is accounted for by stronger acidity of HBF_4 (pKa -0.4) than TFA (pKa 0.23).

Acknowledgements

This work was supported by and Grant-in-Aid for Science Research from the Ministry of Education, Culture, Sports, Science and Technology of Japan.

Notes and references

1 J. Cornil, D. Beljonne, J. –P. Calbert and J.-L. Brédas. *Adv. Mater*., 2001, **13**, 1053.
2 G. Saito and Y. Yoshida, *Bull. Chem. Soc. Jpn*, 2007, **80**, 1.
3 M. V. Peters, R. S. Stoll, A. Kühn and S. Hecht, *Angew. Chem. Int. Ed*., 2008, **47**, 5968.
4 Y. Shirota, *J. Mater. Chem*., 2005, **15**, 75.
5 A Heckmann and C. Lambert. *Angew. Chem. Int. Ed*., 2012, **51**, 326.
6 T. Muraoka, K. Kinbara and T. Aida, *Nature*, 2006, **440**, 512.
7 T. Kato, N. Mizoshita and K. Kishimoto, *Angew. Chem. Int. Ed*., 2006, **45**, 38.
8 A. C. Grimsdale and K. Müllen, *Angew. Chem. Int. Ed*., 2005, **44**, 5592.
9 Freek J. M. Hoeben, Pascal Jonkheijm, E. W. Meijer and Albertus P. H. J. Schenning, *Chem. Rev*., 2005, **105**, 1491.
10 S. Sergeyev, W. Pisulab and Y. H. Geerts, *Chem. Soc. Rev*., 2007, **36**, 1902.
11 C. Joachim, J. K. Gimzewski and A. Aviram, *Nature*, 2000, **408**, 541.
12 R. L. Carroll and C. B. Gorman, *Angew. Chem. Int. Ed.*, 2002, **41**, 4378; E. Amir, R. J. Amir, L. M. Campos and C. J. Hawker, *J. Am. Chem. Soc*., 2011, 133, 10046.
13 K. Kurotobi, K. S. Kim, S. B. Noh, D. Kim and A. Osuka, *Angew. Chem. Int. Ed*., 2006, **45**, 3944.
14 E. Puodziukynaite, H.-W. Wang, J. Lawrence, A. J. Wise, T. P. Russell, M. D. Barnes and T. Emrick. *J. Am. Chem. Soc*., 2014, **136**, 11043.
15 S. Hirakawa, J. Kawamata, Y. Suzuki, S. Tani, T. Murafuji, K. Kasatani, L. Antonov, K. Kamada and K. Ohta, *J. Phys. Chem. A,* 2008**, 112**, 5198.
16 Y. Yamaguchi, K. Ogawa, K.-i. Nakayama, Y. Ohba and H. Katagiri, *J. Am. Chem. Soc*., 2013, **135**, 19095.
17 T. Zielinski, M. Kędziorek and J. Jurczak, *Chem. –Eur. J*., 2008, **14**, 838.
18 T. Nakae, T. Kikuchi, S. Mori, T. Okujima, T. Murafuji and H. Uno, *Chem. Lett*., 2014, **43**, 504.
19 M. Iyoda, K. Sato and M. Oda, *Tetrahedron Lett*., 1985, **26**, 3829.
20 T. Shoji, S. Ito, K. Toyota, M. Yasunami and N. Morita, *Tetrahedron Lett*., 2007, **48**, 4999.
21 S. Ito, H. Inabe, T. Okujima, N. Morita, M. Watanabe, N. Harada and K. Imafuku, *J. Org. Chem*., 2001, **66**, 7090.
22 S. Ito, A. Nomura, N. Morita, C. Kabuto, H. Kobayashi, S. Maejima, K.Fujimori and M. Yasunami, *J. Org. Chem*., 2002, **67**, 7295.
23 F. Wang, T. T. Lin, C. He, H. Chi, T. Tang and Y.-H. Lai, *J. Mater. Chem*., 2012, **22**, 10448.
24 S. C. Lee, A. Ueda, H. Kamo, K. Takahashi, M. Uruichi, K. Yamamoto, K. Yakushi, A. Nakao, R. Kumai, K. Kobayashi, H. Nakao, Y. Murakami and H. Mori, *Chem Comm*., 2012, **48**, 8673.
25 A. Ueda, S. Yamada, T. Isono, H. Kamo, A. Nakao, R. Kumai, H. Nakao, Y. Murakami, K. Yamamoto, Y. Nishio and H. Mori, *J. Am. Chem. Soc*., 2014, **126**, 12184.
26 S. Wakabayashi, Y. Kato, K. Mochizuki, R. Suzuki, M. Matsumoto, Y. Sugihara and M. Shimizu, *J. Org. Chem.*, 2007, **72**, 744; K. Kurotobi, M. Miyauchi, K. Takakura, T. Murafuji and Y. Sugihara, *Eur. J. Org. Chem*., 2003, 3663.
27 M. Grabau, J. Forster, K. Heussner and C. Streb, *Eur. J. Inorg. Chem.*, 2011, 1719.
28 A. M. Spackman and D. Jayatilaka, *CrystEngComm*, 2009, **11**, 19.

We report the synthesis and acid-base property of 1,1'-bi(2-pyridylazulene) and crystal structure of its mono-protonated form in which pyridyl moieties are interacted by intramolecular hydrogen bond.